Adsorption (2013) 19:49–61
DOI 10.1007/s10450-012-9411-5

Preparation and characterization of double metal-silica sorbent for gas filtration

Ebenezer Twumasi Afriyie · Peter Norberg · Christer Sjöström · Mikael Forslund

Received: 13 December 2010 / Accepted: 22 August 2012 / Published online: 6 September 2012
© Springer Science+Business Media, LLC 2012

Abstract This paper presents the preparation of a porous (Mg, Ca) silicate structure, which could be employed as sorbent filter media. The sorbents have been prepared using sodium silicate precipitated with various ratios of magnesium and calcium salts. The sorbents obtained were characterized using scanning electron microscope (SEM), X-ray diffraction (XRD) and nitrogen physisorption isotherm. Further, the applicability and performance of the sorbent impregnate with potassium hydroxide for removal of sulphur dioxide (SO_2) has been demonstrated. From the isotherms, specific surface area, pore diameter and volume of pores were estimated. Results show that the chemical composition and textural properties of the resultant sorbents were highly dependent on Mg/Ca molar ratio. It was found that sorbents made with 68 mol% Mg and 32 mol% Ca (PSS-MgCa-68/32); and 75 mol% Mg and 25 mol% Ca (PSS-MgCa-75/25) exhibited even higher specific surface area and pore volume than the sorbents containing a single metal. The Mg/Ca-silica sorbents obtained contains interconnected bimodal porosity with large portions being mesopores of varied sizes. The pore size distribution (PSD) results further indicate that PSS-MgCa-68/32 sorbent exhibits wide PSD of interconnected pores in the size range of 1 to 32 nm while PSS-MgCa-50/50 and PSS-MgCa-75/25 exhibits narrow PSD of 1 to 5 nm. Using SO_2 as model contaminate gas, it was shown that the dynamic adsorption performance of the PSS-MgCa-sorbents impregnated with 8 wt% KOH exhibits SO_2 uptake, with impregnated PSS-MgCa-68/32 showing better performance. This shows that the materials prepared can be used as adsorbent for gas filtration.

E. Twumasi Afriyie (✉) · P. Norberg · C. Sjöström · M. Forslund
Materials Technology, KTH Research School, University of Gävle, Gävle, Sweden
e-mail: ebenezer.twumasi@hig.se

Keywords Mg/Ca-silica sorbent · Gas filtration · Characterization · Textural properties · Impregnate Mg/Ca-silica sorbents

Abbreviations

d_{mes}	maximum mesopores size distribution
d_{mic}	maximum micropores size distribution
NLDFT	Nonlocal Density Functional Theory
p/p°	Relative pressure
PSD	Pore Size Distribution
S_{BET}	Specific Surface area obtained via Brunauer-Emmet-Teller-equation
S_{mes}	Mesoporous surface area obtained via t-plot
S_{mic}	Micropore surface area obtained via t-plot
V_{mes}	Mesoporous pore volume obtained via t-plot
V_{mic}	Microporous pore volume obtained via t-plot
V_{tot}	Total pore volume
XRD	X-Ray-Diffraction

1 Introduction

In the current industrial society, the atmospheric concentrations of gases such as CO_2, CO, CH_4, and N_2O (greenhouse gases), NO_x, SO_2 and H_2S have, for various reasons, attracted attention. These gases are believed to be a major contributor of acid rain, global warming and increased toxicity of breathing air (Finlayson-Pitts and Pitts 1986).

There are known ways to capture the emissions of these gases, but only adsorption has found widespread use (John et al. 2000; Schweitzer 1979). The performance of the adsorption process depends on the quality of the adsorbent used. At present the most generic adsorbents used commercially are activated carbon, activated alumina, molecular

sieve and silica gel (Schweitzer 1979; Yang 2003). Considering the global environmental movement for clean air as well as rapid growth of developing countries, the development of new and better sorbents will not only make major advances in gas adsorption technology but also meet new challenges that cannot be met with the sorbents that are currently available.

Ordered mesoporous silicas have recently been synthesized using surfactant as templates. These mesoporous silicas exhibits high surface area and narrow pore size distribution in the meso range. These properties have led to their study for applications in fields such as molecular sieving, catalysis, selective adsorption of pollutant gases and so on (Zheng et al. 2007). However, industrial applications of the mesoporous materials have been inhibited by surfactants toxicity and high cost (Lu 2004), low hydrothermal stability such as in boiling water and mechanical stability (Ryoo et al. 1996; Bonneviot et al. 1998). For example the disintegration of MCM-41 and MCM-48 during impregnation in aqueous solutions and collapse of frameworks during the attempt to pelletize with compression above 1000 kg cm^{-1} has been reported (Bonneviot et al. 1998). These drawbacks provoke a doubt about its durability in practical application. Herein we focus on route of synthesis of mesoporous silica without surfactant in which impregnate chemical can be incorporated into their pore systems without being destroyed. In this work calcium chloride and magnesium chloride have been used to precipitate the silica instead of using surfactants. Comprehensive studies on the use of the sodium ion, ammonium salts, the calcium ion and other polyvalent metal ions to precipitate silica have been reported by several groups and summarized by (Iler 1979). The properties and use of synthetic calcium silicate and magnesium silicate as sorbent has been investigated and reported by several groups (Renedo and Fernández 2002; Lin et al. 2003; Taspinar and Ozgul-Yucel 2008; Ciesielczyk et al. 2007; Odler 2003). However, the use of both calcium and magnesium salts as precipitating agents have not been reported in this context. To the best of our knowledge only M.S. Ahmed and Y.A. Attia (Ahmed and Attia 1998) have reported on the synthesis of aerogel containing both CaO and MgO. In their preparation, they first prepared alcogel by the sol-gel process and finally dried the alcogel at supercritical temperature (Ahmed and Attia 1998). Their aim was to synthesize aerogel structure containing CaO and MgO for removal of greenhouse gases and acidic gases. Their synthesis route did not allow impregnation of the aerogel to increase its removal performance. To avoid high costs associated with the TEOS (tetraethyl orthosilicate) and the high pressure process linked with supercritical drying (Pierre and Pajonk 2002), the present work has been aimed at the use of water glass (sodium silicate) and calcium and magnesium salts to synthesize mesoporous sorbent containing CaO and MgO. The effect of various Mg/Ca molar ratios on the structural, morphological and textural properties of the mesoporous sorbents prepared was studied by using scanning electron microscopy (SEM), X-ray diffraction (XRD) and nitrogen adsorption/desorption isotherms. From the adsorption isotherms, specific surface area (S_{BET}), pore diameter (d_{mic} and d_{mes}) and total volume of pores (V_{tot}) were estimated.

The dynamic adsorption performance of the sorbents impregnated with potassium hydroxide was tested by subjecting the materials to a challenge air stream containing 3100 ppb of SO_2. In some of the challenge tests, a commercial alumina, impregnated with 8 %wt $KMnO_4$ was also included, in this case CamPure 8 or CP8 as abbreviated in the graphs. Non-carbon filter media are particularly interesting in applications where non-combustible materials are required, e.g. in oil refineries and petrochemical plants. The inclusion of CamPure 8 in some of the gas adsorption tests only serves as a marker for a typical commercial filter medium belonging to this class of materials, as are also the experimental materials of this investigation.

2 Experimental

2.1 Synthesis of sorbent

Sorbents were prepared from waterglass (SiO_2/Na_2O = 3.35) as silica source, $MgCl_2{\cdot}6H_2O$ and $CaCl_2{\cdot}2H_2O$ salts as magnesium and calcium sources, respectively. The silica content was maintained constant but the moles of $CaCl_2$ and $MgCl_2$ salts were varied. A 500 ml salt solution of either pure 0.43 mol $CaCl_2$ or pure 0.43 mol $MgCl_2$ was prepared or mixtures of said solutions in ratios indicated in Table 1. The synthesis was done by pouring 500 ml salt solution into a 1.5 M (with respect to SiO_2) sodium silicate solution (500 ml), which was being agitated in an ordinary food mixer at room temperature. The resulting solution immediately began to coagulate. The reaction is assumed to occur according to the following reaction formula:

$$\mathrm{Na_2O{\cdot}nSiO_2\ (l)} + 1/2\mathrm{Mg^{2+}} + \frac{1}{2}\mathrm{Ca^{2+}} \rightarrow \left(\frac{1}{2}\mathrm{Mg}, \frac{1}{2}\mathrm{Ca}\right)\mathrm{O{\cdot}nSiO_2\ (s)} + 2\mathrm{Na^{+}} \quad (1)$$

The reaction yielded a white coagulum and was allowed to settle for up to one hour and the clear liquid above the precipitated coagulum was removed by decanting. Then, the coagulum was mixed with a defined amount of water followed by stirring, settling and decanting as before. This step was repeated a number of times until the decanted liquid was virtually free from chloride ions as detected by adding a few drops of dilute $AgNO_3$ reagent to the decanted liquid. The

coagulum obtained after the final washing was vacuum filtered through filter paper until a paste holding as much as 85 % of water was obtained. The sample obtained was made into pellets and subsequently dried overnight in a stationary dryer at 105 °C. The Precipitated Silica Sorbent obtained were designated by an abbreviation; e.g. a sorbent made by 100 mol % Mg will be called PSS-MgCa-100/0, 75 mol% Mg and 25 mol% Ca will be PSS-MgCa-75/25, 68 mol% Mg and 32 mol-% Ca will be PSS-MgCa-68/32, 50 mol-% Mg and 50 mol-% Ca will be called PSS-MgCa-50/50, and 100-mol% Ca will be called PSS-MgCa-0/100. The procedure involving the preparation of the sorbents and textural properties determination were repeated two times.

2.1.1 Impregnation

8 wt% potassium hydroxide (KOH) was added as impregnate chemical to the PSS-MgCa coagulum in the form of powder which subsequently were dissolved in the remaining (85 %) water phase of the coagulum and stirred for 30 min. The weight percentage of KOH has been calculated based on the dry weight of the coagulum. The resultant slurry is formed into pellets and dried at 105 °C.

2.2 Materials characterization

X-ray diffraction studies X-ray diffraction measurements were performed on a Bruker AXS D8 Advance diffractometer equipped with a secondary monochromator and automatic divergence slits (filtered Cu-Kα radiation, 40 kV, 40 mA, wavelength 1.54056 Å). The diffraction patterns were recorded between 5–70° 2θ using a step size of 0.01° and count time per step of 1 s.

Scanning electron microscopy SEM images were obtained using a Hitachi S-3000N SEM (Hitachi, Japan) at an acceleration voltage of 2 kV or 4 kV. The images were recorded on samples with no sputtered coating. The elemental analysis was done with an energy dispersive detector (EDX) equipped in the SEM.

Nitrogen adsorption studies: The adsorptive properties of the sorbents prepared were studied by nitrogen adsorption at 77 K using a Micromeritics ASAP 2010. The adsorption was measured starting from the relative pressure $p/p^\circ \approx 2.87 \times 10^{-4}$ up to $p/p^\circ \approx 0.99$. Before the analysis, all the samples were degassed under vacuum for 20 hours at 150 °C. The built-in automatic leakage test of the ASAP equipment was used as a means to ensure the sample was virtually free from moisture and other adsorbed gases. The specific surface area (S_{BET}) was calculated using the standard BET equation. This was evaluated using nitrogen adsorption isotherm data in the relative pressure (p/p°) range from 0.05 to 0.3. The total pore volume (V_{tot}) was estimated on the basis of the amount adsorbed at $p/p^\circ \approx 0.99$. Pore size distributions (PSD) were derived using the density functional theory method (DFT). The models adopted for the sorbents prepared were non-local density functional theory (NLDFT) for pillared clay model and N_2–Cylindrical Pores-Oxide surface model. Cylindrical pore geometry was assumed for both models. The selected model is applied over the entire range of the adsorption branch of the isotherm and is not restricted to a limited range of relative pressure or pore size. PSD is calculated by fitting to a theoretical set of adsorption isotherms, evaluated for different pore sizes, to the experimental results. For example Fig. 1 shows the experimental N_2 adsorption isotherm together with the NLDFT best fitting isotherm for PSS-MgCa-68/32 sample.

Dynamic SO_2 adsorption The performance of impregnated samples was tested by subjecting them to dynamic adsorption of SO_2 at ppb level. It is worth noting that the adsorbents prepared or obtained were used without degassing to reflect a real life scenario. The analysis was performed in a system similar to the setup in ASHRAE 145.1 (2008). A typical molecular filter for SO_2 adsorption may consist of a bed shaped compartment made of perforated plates into which adsorbents are packed. An air stream polluted with low concentrations of SO_2 is forced through the bed via the perforated plates and the SO_2 are adsorbed. In this analysis four comparable samples of grams each were loaded into four parallel columns forming 26 mm high beds. The inlet air contaminated with 3100 ppb SO_2 at 23 °C and 50 % RH was made to pass through the columns. The air with controlled temperature and humidity is fed from a large supply chamber and the selected challenge gas is injected from a pressurized gas cylinder by means of a computer controlled mass flow valve. The SO_2 is measured by a Thermo Environmental 43 C UV fluorescence instrument with a TE 340 H_2S converter. The flow rate of the contaminated air was 30 l/min and the contact time 0.1 s. The concentration of SO_2 was measured up-stream of the samples and directly after each of the columns containing the samples. The removal efficiency [%] in relation to adsorbed amount in grams was also calculated. The schematic SO_2 adsorption challenge test setup used in this study is shown in Fig. 2.

3 Results and discussion

3.1 X-ray diffraction

Measurement at low-angle (1–5°) did not produce any distinctive peak which indicates short range order or disordered phases present in the all samples prepared. The wide-angle powder X-ray diffraction patterns of all samples prepared are shown in Fig. 3. All the samples exhibits broad peaks centered at 2θ value of around 20–30° which is consistent

Table 1 Chemical composition of sorbents in relation to sodium silicate (1.5 M SiO_2) molar ratio 3.35 precipitated with various Mg- and/or Ca-molar ratios

Samples	Pre-mixing condition		Chemical composition of sorbent			Mean Si/(Mg+Ca)
	Mg^{2+} mol%	Ca^{2+} mol%	Si atom%	Mg atom%	Ca atom%	
PSS-MgCa-0/100	0	100	26.4	0	10.4	2.5
PSS-MgCa-50/50	50	50	27.2	3.9	5.4	2.9
PSS-MgCa-68/32	68	32	27.8	5.3	3.0	3.3
PSS-MgCa-75/25	75	25	27.6	6.0	2.4	3.3
PSS-MgCa-100/0	100	0	25.2	7.4	0	3.4

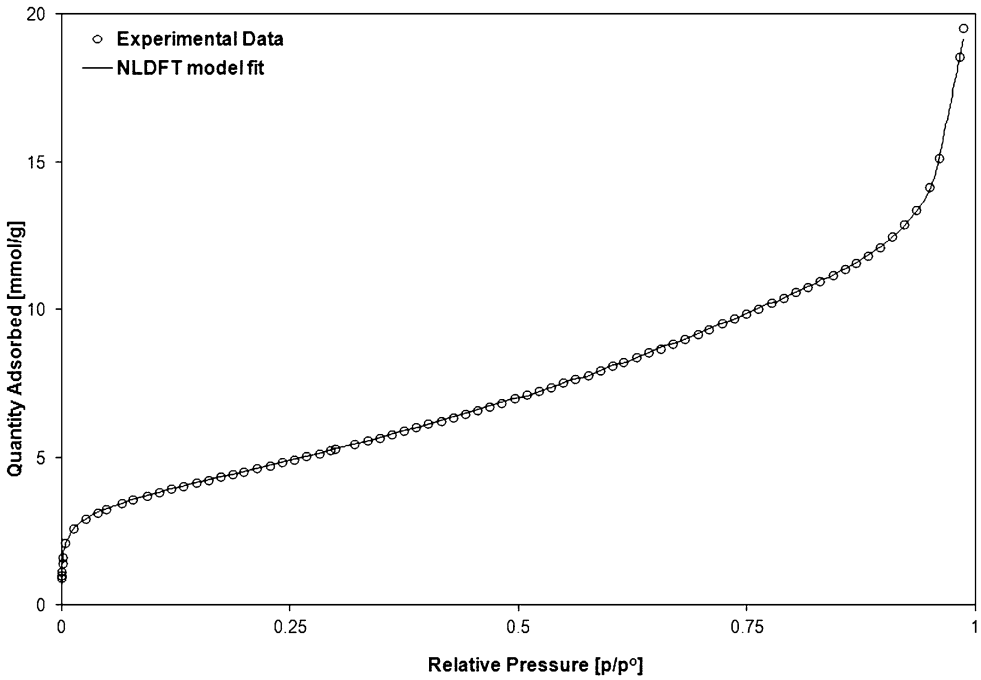

Fig. 1 Experimental N_2 adsorption isotherm and NLDFT model best fitting isotherm for PSS-MgCa-68/32

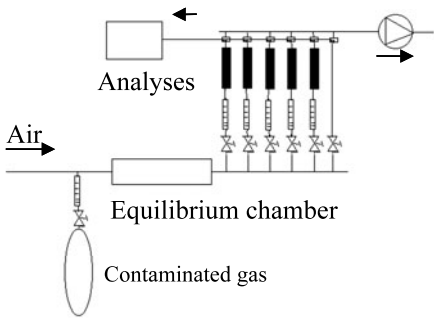

Fig. 2 Schematics SO_2 challenge test setup

with typical amorphous nature of the silica. The small peaks observed in the PSS-MgCa-0/100 indicate the presence of small amounts of crystalline compounds but the exact compounds could not be identified. Further weak peaks were also observed in PSS-MgCa-50/50. Thus as the mol% of Ca decreases and mol% Mg increases, the characteristic peaks of crystalline compounds becomes weaker, and invisible as the Ca mol% become less than 50 and the Mg mol% more than 50, whereas instead the characteristic hump of silica becomes more marked.

3.2 Scanning electron microscopy

The elemental composition of the sorbents, determined by energy dispersive detector in SEM is reported in Table 1. The analysis was done to see if the Mg^{2+} and Ca^{2+} were able to replace $2Na^{+}$ in the (Na_2O $nSiO_2$) as given by the reaction (1). The sorbents prepared had mean Si/(Mg+Ca) ratios in the range of 2.5–3.4, a range very close to the SiO_2/Na_2O molar ratio of 3.35. This may indicate that (Mg, Ca) O was formed and replaced the Na_2O in the ($Na_2O{\cdot}nSiO_2$) in the final sorbent produced. Figure 4 displays SEM micrographs of the sorbents prepared. The micrographs show that all the sorbents prepared are composed of primary particle sizes, which are very small and platelike

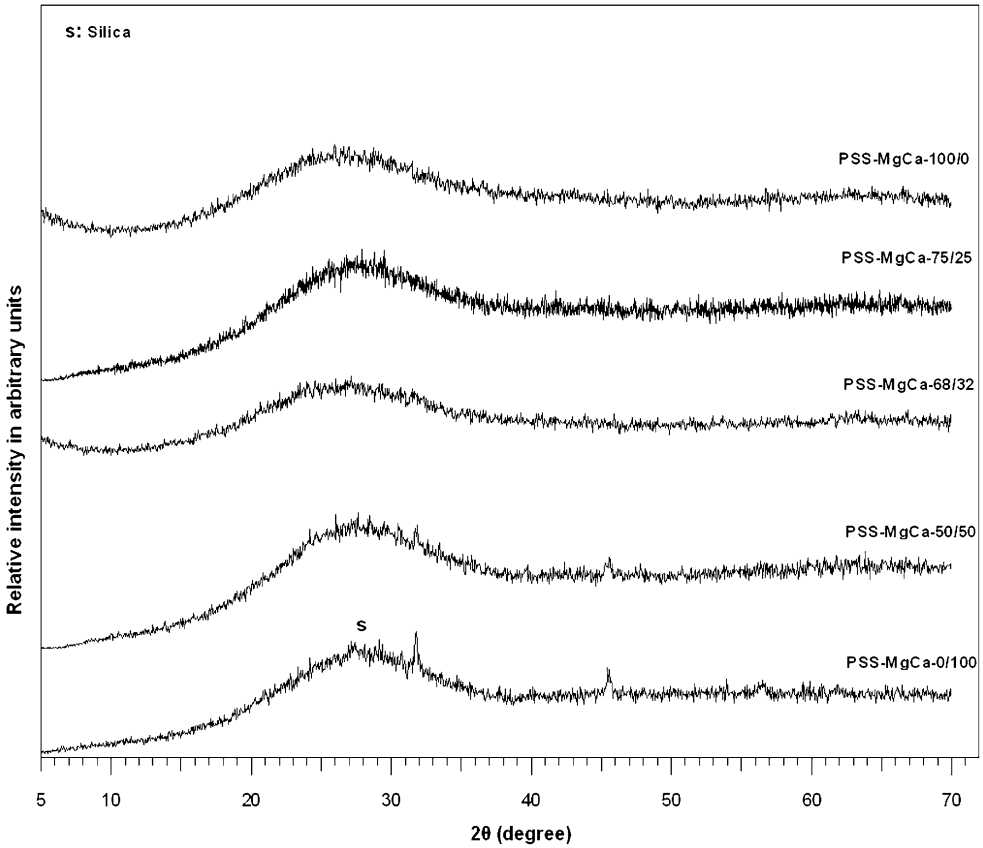

Fig. 3 XRD patterns of sorbents prepared with various Mg- and/or Ca molar ratios

which tend to cohere to form a porous structure. Sorbents prepared with single Ca metal are observed to be composed of more compact particles whereas the corresponding sample made with 100 mol% Mg (PSS-MgCa-100/0) show plate particles that are more porous in nature. Further magnification reveals that PSS-MgCa-75/25 was made of small agglomerates of platy particles. In case of PSS-MgCa-68/32, a monolith made of particles that are smaller and more homogeneous in size was observed.

3.3 Nitrogen physisorption

3.3.1 Surface area and pore volume

The adsorptive properties of the sorbents prepared have been studied by nitrogen adsorption. Nitrogen adsorption isotherms of all sorbent samples with various Mg/Ca mol% are presented in Fig. 5A and the corresponding physicochemical parameters are summarized in Table 2. All the sorbent samples prepared yields completely reversible type IIb isotherm with a clear type-H3 hysteresis loop based on IUPAC classification (Rouquerol et al. 1996). An adsorption at very low relative pressure, $p/p^\circ < 0.1$ was observed for all the samples prepared indicating the presence of some micropores in the samples. The increase in nitrogen adsorption at low pressure was more pronounced in PSS-MgCa-100/0 followed by that of PSS-MgCa-75/25. The PSS-MgCa-0/100 exhibited lowest uptake of nitrogen at low relative pressure. For sorbents with both Mg/Ca it was observed that the nitrogen uptake at low relative pressure begins to increase when the mol% of Mg is 50 % or more. The uptake at low p/p° then increases accordingly as the Mg mol% increases to 100.

The shape of the hysteresis loop (Type-H3) can be attributed to development of a network of slit-shaped pores with varied sizes or to agglomerates of platy particles (Rouquerol et al. 1996). Several models have suggested that the calcium silicate hydrate gel consists of very thin sheets (Jennings et al. 2008). Such sheets in the samples prepared may well produce plate-like or slit-shaped pores. A sharp rise in nitrogen uptake at higher relative pressures was observed amongst all the samples prepared. The very small hysteresis loop above $p/p^\circ \approx 0.9$ in their isotherms is a sign of condensation in intraparticle of colloidal-size silica. The nitrogen adsorption uptake at both low and high relative pressure was found to be sensitive to changes of the Mg/Ca molar ratio. It can be seen from Fig. 5A that PSS-MgCa-68/32 which has lower nitrogen uptake at low relative pressure range compared with samples made with ≥ 75 mol% Mg, did adsorb more nitrogen at high relative pressure range. Furthermore, the effect of 68 mol% Mg/32 mol% Ca on the pore structure provides evidence in the appear-

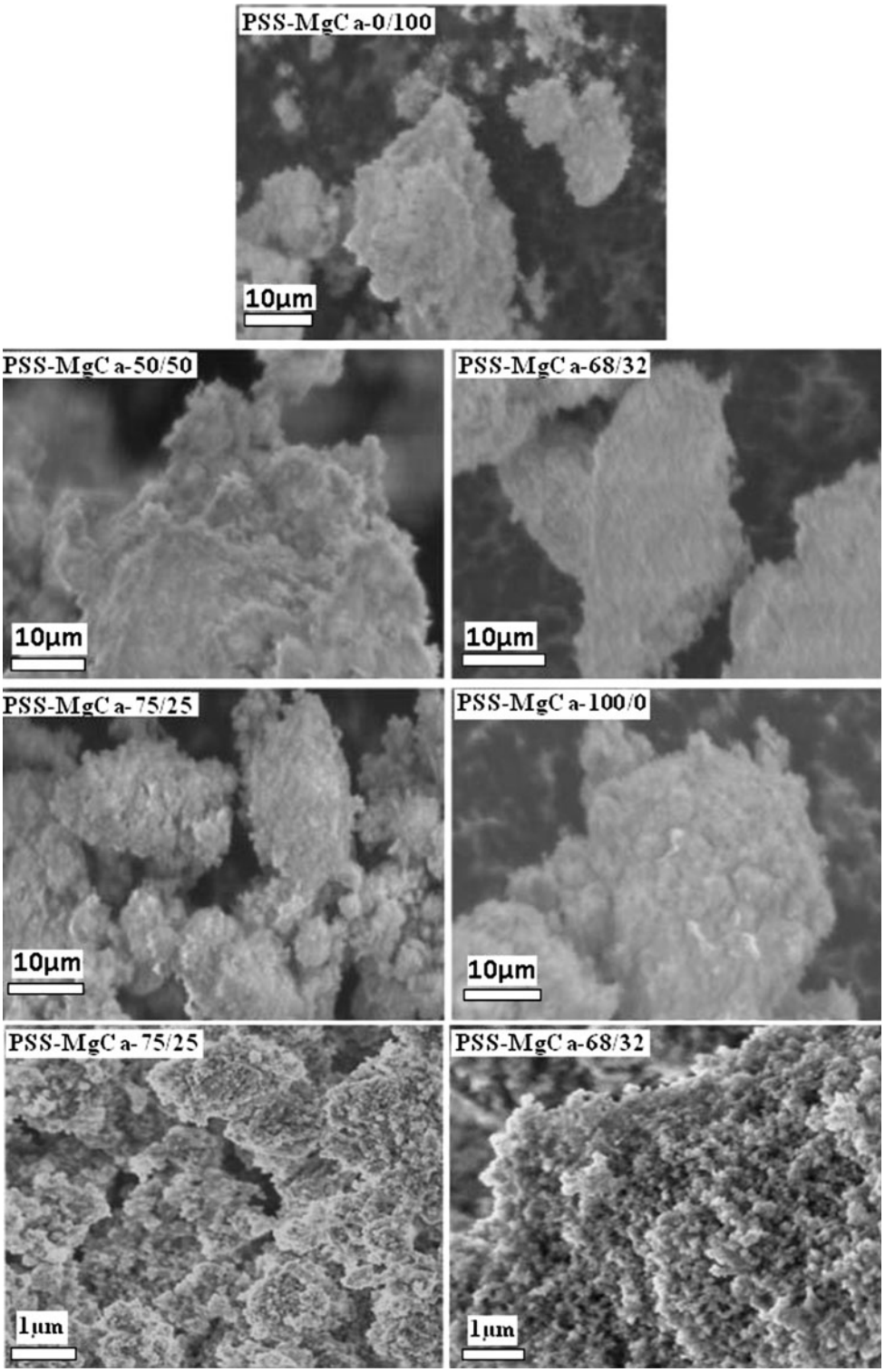

Fig. 4 SEM micrographs of sorbents prepared with various Mg- and/or Ca molar ratios

ance of its hysteresis loop in which a small sharp step in the amount desorbed at about $p/p^\circ = 0.40$ and wide hysteresis loop was observed. Sharp steps in 77 K nitrogen adsorption isotherms of homogeneous mesoporous silica materials around $p/p^\circ = 0.3$ are commonly observed (Kruk and Jaroniec 1997). PSS-MgCa-68/32 material exhibits heterogeneity of mesopore size distribution as evidenced by gradual shift of p/p° value in the same region as indicated in Fig. 5A. The observed wide hysteresis loop indicates the presence of interconnected meso pores in a broad size range. These features were not exhibited by the rest of the samples.

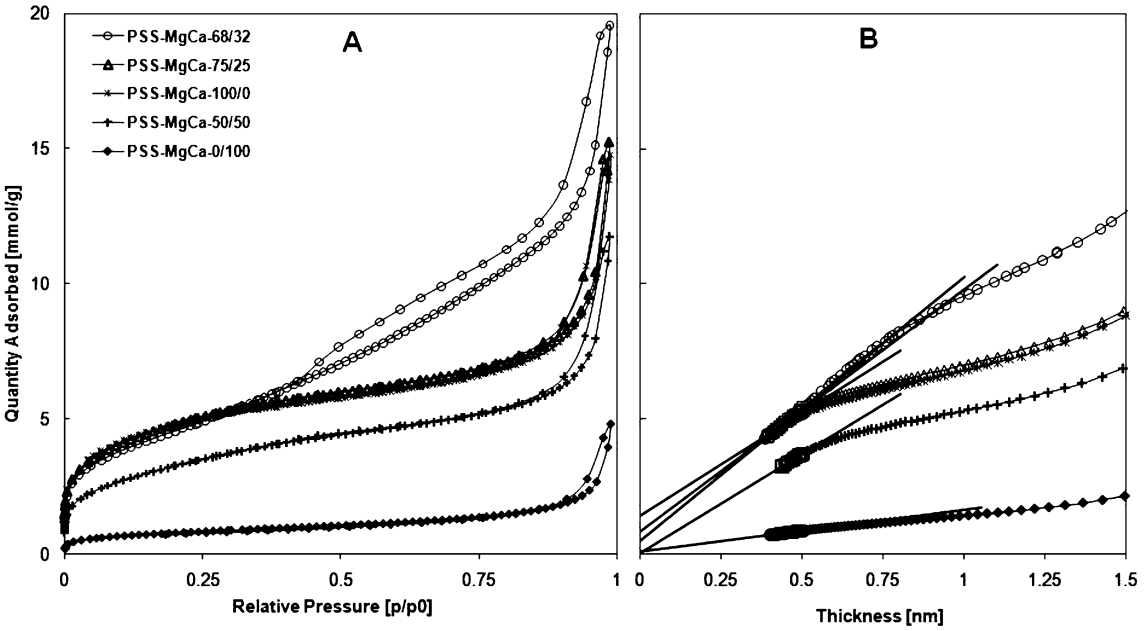

Fig. 5 Nitrogen adsorption-desorption isotherms (**A**) and (**B**) *t*-plot of sorbents prepared with various Mg- and/or Ca molar ratios

Table 2 Textural properties of sorbents prepared with various Mg- and/or Ca molar ratios and sorbents impregnated with 8 wt% KOH

Samples	S_{BET} (m^2/g)	S_{mic} (m^2/g)	S_{mes} (m^2/g)	V_{tot} (cm^3/g)	V_{mic} (cm^3/g)	V_{mes} (cm^3/g)	d_{mic} (nm)	d^{HK} (nm)	d_{mes} (nm)
PSS-MgCa-0/100	63	9.0	53.6	0.17	0.003	0.167	1.40	1.33	2.4
PSS-MgCa-0/100	64	10	54	0.22	0.005	0.215	1.40	1.33	2.4
PSS-MgCa-50/50	267	13	254	0.41	0.003	0.408	1.37	1.33	2.3
PSS-MgCa-50/50	259	12	247	0.43	0.004	0.426	1.37	1.33	2.3
PSS-MgCa-50/50-KOH	221	6	215	0.55	0.003	0.547	1.61	1.41	25.4
PSS-MgCa-68/32	373	45	328	0.65	0.021	0.625	1.41	1.29	5.4
PSS-MgCa-68/32	372	49	323	0.63	0.020	0.610	1.41	1.29	5.4
PSS-MgCa-68/32-KOH	312	30	282	0.59	0.012	0.578	1.41	1.29	5.4
PSS-MgCa-75/25	374	66	308	0.53	0.031	0.499	1.36	1.28	2.4
PSS-MgCa-75/25	371	60	311	0.52	0.030	0.490	1.36	1.28	2.4
PSS-MgCa-75/25-KOH	361	23	338	0.58	0.009	0.571	1.71	1.47	3.5
PSS-MgCa-100/0	368	113	255	0.51	0.054	0.456	1.40	1.17	2.4
PSS-MgCa-100/0	347	109	238	0.55	0.046	0.504	1.40	1.17	2.4
PSS-MgCa-100/0-KOH	320	19	227	0.22	0.010	0.21	1.70	1.57	3.7

S_{BET}—BET specific surface area, S_{mic}—*t*-plot micropore surface area, S_{mes}—mesopore surface area, V_{tot}—total pore volume, V_{mic}—micropores volume, V_{mes}—mesopores volume, d_{mic}, d_{mes}—micro-and mesopore maxima peaks in DFT pore size distribution, d^{HK}—micropore pore size obtained from Horvath-Kawazoe (H-K) equation

The uptake of nitrogen was highest at high p/p° range and increased in the order: PSS-MgCa-0/100 < PSS-MgCa-50/50 < PSS-MgCa-100/0 < PSS-MgCa-75/25 < PSS-MgCa-68/32.

It is evident that varying the Mg/Ca ratio has an influence on the physicochemical parameters of the sorbents prepared. From Table 2 it can be observed that samples made with 100 mol% Ca (PSS-MgCa-0/100) exhibits low S_{BET} whereas the corresponding sample made with 100 mol% Mg (PSS-MgCa-100/0) show a significantly higher S_{BET}. It may also be noted that for sample made with 68 % Mg and 32 % Ca (PSS-MgCa-68/32); 75 mol% and 25 mol% Ca (PSS-MgCa-75/25) exhibited even higher S_{BET} than the samples containing the single metal. The S_{BET} of PSS-MgCa-68/32 and PSS-MgCa-75/25 are nearly the same, and have a better S_{BET} compared with the rest of the samples prepared. The

S_{BET} of the samples decreased from 373 m^2/g (PSS-MgCa-68/32) to 257 m^2/g (PSS-MgCa-50/50) when Ca content was 50 mol% and it continues to dramatically decrease to 63 m^2/g (PSS-MgCa-0/100) when Ca content was 100 mol%. The change of specific surface area with the Mg/Ca ratio can be explained by referring to the XRD analysis. It can be observed from Fig. 3 that samples that exhibited crystalline compounds show less S_{BET} (Table 2).

Lin and co-workers (Lin et al. 2003) prepared $3CaO{\cdot}2SiO_2{\cdot}4H_2O$ sorbents with various ratios of Ca/SiO_2. It was shown that particles of the sorbent were composed of either open structure thin foils of $3CaO{\cdot}2SiO_2{\cdot}4H_2O$ or some particles were more compact or sorbent compose of both particles based on the Ca/SiO_2 ratio. Magnesium silica hydrates have been shown to consist of agglomerates of thin plate particles (Brew and Glasser 2005). In this experiment, the formation of compact plate like particles of calcium silicate hydrate was more abundant in the sample prepared with 100 mol% Ca and therefore reducing the accesses of nitrogen into some of the pores.

This can be partly explained by the higher atomic weight of Ca. When the Ca mol% is reduced to 50 and Mg increased to 50 mol%, the amount of compact particles of $3CaO{\cdot}2SiO_2{\cdot}4H_2O$ is reduced and the introduction of Mg results in the formation of porous agglomerates of magnesium silicate particles in the sorbent consequently increases the surface area and the volume of pores. For the PSS-MgCa-68/32 sorbent the amount of magnesium silicate increased and the S_{BET} increased accordingly. According to the results in Table 2, the V_{tot} follow the same pattern as does the S_{BET} with the exception of PSS-MgCa-75/25, which had similar S_{BET} as PSS-MgCa-68/32, but the results of the V_{tot} was contrary to the S_{BET}.

The amount of micro- and mesopores in the sorbents has been calculated via *t*-plots by Harkins and Jura equation (Rouquerol et al. 1996) with thickness range of 0.4 nm to 0.5 nm. The *t*-plots are shown in Fig. 5B and the corresponding parameters shown in Table 2. The presence of micropores in the sorbents prepared is confirmed by the fact that the linear region of the *t*-plot intercepts the y-axis in these plots. The micropore volumes (V_{mic}) of the samples are derived from the y-axis intercept of the extrapolated linear region and mesoporous area (S_{mes}) from the slope in these plots. Given this, the V_{mic} and S_{mic} of sorbents with $\geq$75 mol% of Mg are relatively large compared with the rest of the samples. The S_{mic} contributions to the respective S_{BET} are for PSS-MgCa-0/100: 14 %, PSS-MgCa-50/50: 5 %, PSS-MgCa-68/32: 12 %, PSS-MgCa-75/25: 18 % and PSS-MgCa-100/0: 30 %. The V_{mic} follows similar pattern as does the S_{mic}. It can be concluded that the sorbents prepared have mesopores occupying large portions of their pore system.

It is worth noting that PSS-MgCa-68/32 has a relatively large S_{mes} and V_{mes} compared with the rest of the samples. This can be explained by the fact that PSS-MgCa-68/32 from SEM image has it constituent primary particles size being very small and homogeneous. Therefore the mesopores originated from intraparticle spaces created between the primary particles is much more distributed throughout the structure than the rest of the samples.

3.3.2 *Pore size distribution*

Due to the amorphous nature of the sorbents, no structural data related to the pore size could be obtained by XRD and therefore the pore structure properties have been obtained by physisorption isotherms that are able to differentiate between micro and mesoporosity. Pore size distribution (PSD) curves, as derived by DFT methods are displayed in Fig. 6. The pore diameter values taken as the maximum peak of the PSD curve are listed in Table 2. Pore size analysis based on DFT calculations is only applicable if the theoretical set of models fit the experimental set of adsorption isotherm data (Fig. 1). Therefore the assumption of models must reflect the isotherm shape and the pore shape and the physical/chemical nature of the pore surface. In this work two models have been assumed for the sorbents; NLDFT Pillared Clay model and N_2–Cylindrical Pores-Oxide surface model. For both models cylindrical geometry was assumed. The assumptions were based on the fact that the sorbent isotherms appear to have the same typical type II character as is often associated with the nitrogen isotherm on pillared clays (Rouquerol et al. 1996). Further the chemical composition and images from the SEM indicates the presence of plate–like particles composed of CaO and MgO in the sorbent.

It is interesting to note that both N_2–Cylindrical Pores-Oxide surface model and NLDFT Pillared Clay model fit the experimental adsorption isotherms of all the samples made with various Mg/Ca mol%. Nevertheless both cases give similar values of pore size. One can observe that when using N_2–Cylindrical Pores-Oxide surface model, sharp peaks appeared in the micropore size range and a less sharp or broad peak in the mesopore size range (see Fig. 6). However, when the NLDFT Pillared Clay model is assumed, reverse results are obtained. It is evident from these results that the sorbent made with various Mg/Ca mol% contains micropore of cylindrical shape and mesopore pillared clay-like shape and probably other irregular pore shapes.

To verify the possibility of other pore geometries in the prepared samples, N_2-DFT model with slit pore geometry was assumed. In this case, the model isotherm did not fit the experimental isotherms of the sorbents prepared. This indicates that the use of cylindrical pore geometry with the N_2–Cylindrical Pores-Oxide surface model and Pillared Clay model to the sorbents prepared is justified due to apparently sufficient similarity in the pore shape and surface properties. From Fig. 6, the sorbents prepared shows interconnected

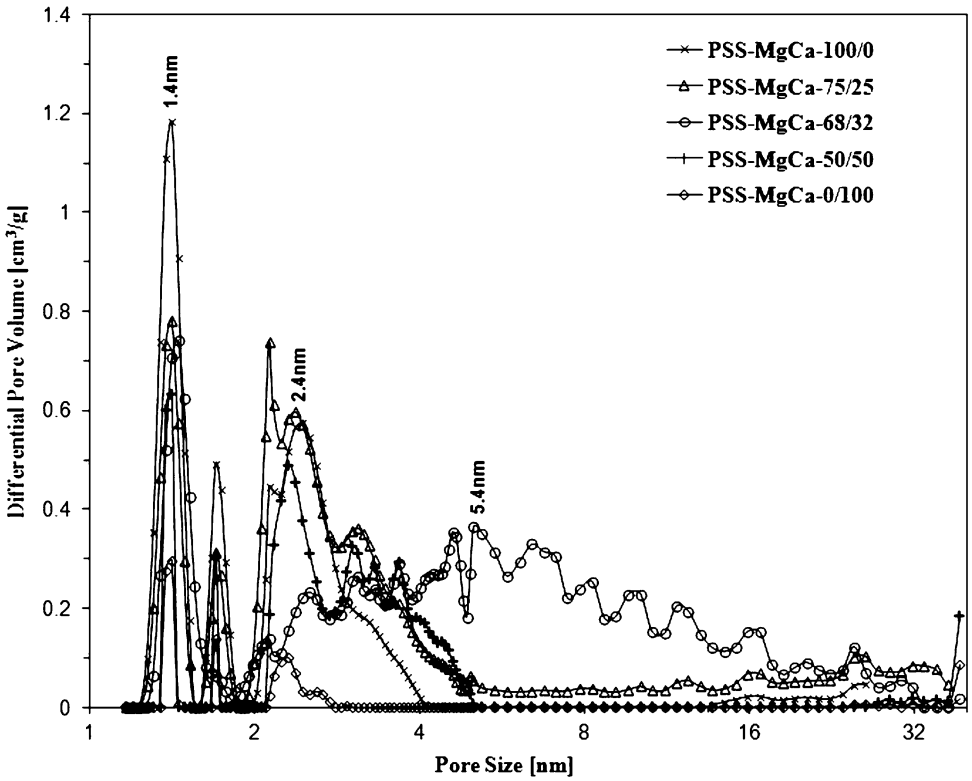

Fig. 6 DFT Pore size distributions of sorbents prepared with various Mg- and/or Ca molar ratios. PSD of all samples have been determined by N_2–Cylindrical Pores-Oxide surface model and assuming cylindrical pore geometry

bimodal pores distribution of micro and mesopore region, PSS-MgCa-50/50 and PSS-MgCa-75/25 exhibited narrow pore size range with micropore diameter centered at about 1.4 nm and mesopore diameter centered at about 2.4 nm, whereas PSS-MgCa-68/32 shows a sharp wide pore size distribution with micropore diameter centered at about 1.4 nm and mesopore diameter at about 5.4 nm.

The PSD of PSS-MgCa-68/32 further confirmed the existence of interconnected heterogeneous mesopore size distribution as observed from wide hysteresis loop in its isotherm. The sharp PSD of PSS-MgCa-68/32 may be due to the fact that pores arise from smaller and homogeneous silica particles as observed in the SEM images. The pores in this case will be quite large. This explains why PSS-MgCa-68/32 shows a wide PSD in the range of 1.4 nm to 32 nm with abundance of pores in the range of 5 nm to 20 nm. On the other hand, PSS-MgCa-75/25, which shows smaller and inhomogeneous particle sizes, exhibits pores in size range of 1.4 nm to 5 nm. The sorbents made with 100 mol% Mg and 100 % Ca also did exhibit a narrow PSD range of 1 to 5 nm with the maximum micropore and mesopore size centered at 1.2 nm and 2.3 nm for PSS-MgCa-100/0 and 1.4 nm and 2.4 nm for PSS-MgCa-0/100 respectively. A similarity observed amongst PSS-MgCa-50/50, PSS-MgCa-68/32 and PSS-MgCa-75/25 is the presence of a sharp peak appearing at a pore diameter centered at ca. 25 nm on the PSD curve. This kind of pores originates from spaces between relatively large particles.

Besides the DFT method, the micropore size distribution for the sorbents has been calculated with the Horvath-Kawazoe (H-K) (Saito-Foley) method from the adsorption branch assuming cylindrical–shaped geometry of the pores (Horvath and Kawazoe 1983). The H-K equation parameters (Larsen et al. 2000) used in this evaluation are given in Table 3. Micropore size distributions obtained for sorbents prepared with different Mg- and or/Ca molar ratio is shown in Fig. 7 and values in Table 2. All the sorbents were found to have micropores having distributions with maxima positions at about 1.17 nm and 1.3 nm and show a very good agreement with the maxima position of micropore size obtained from NLDFT PSD curves. This suggests that the micropore size of the samples prepared can be represented by both cylindrical and pillared clay-like geometries considered in these methods.

3.3.3 Surface and pore volume of impregnate PSS-MgCa sorbents

Table 2 shows the surface area and pore volume of both the virgin and impregnate PSS-MgCa-sorbents. At 8 wt% KOH incorporated into PSS-MgCa-68/32 substrate, there is about 16 % and 7 % reduction of surface area and pore volume, respectively. The isotherms and pore size distributions for impregnated PSS-MgCa-68/32 (see Fig. 8) did not show any significant changes when compared to the starting substrate. On the other hand, incorporation of 8 wt% KOH did affect

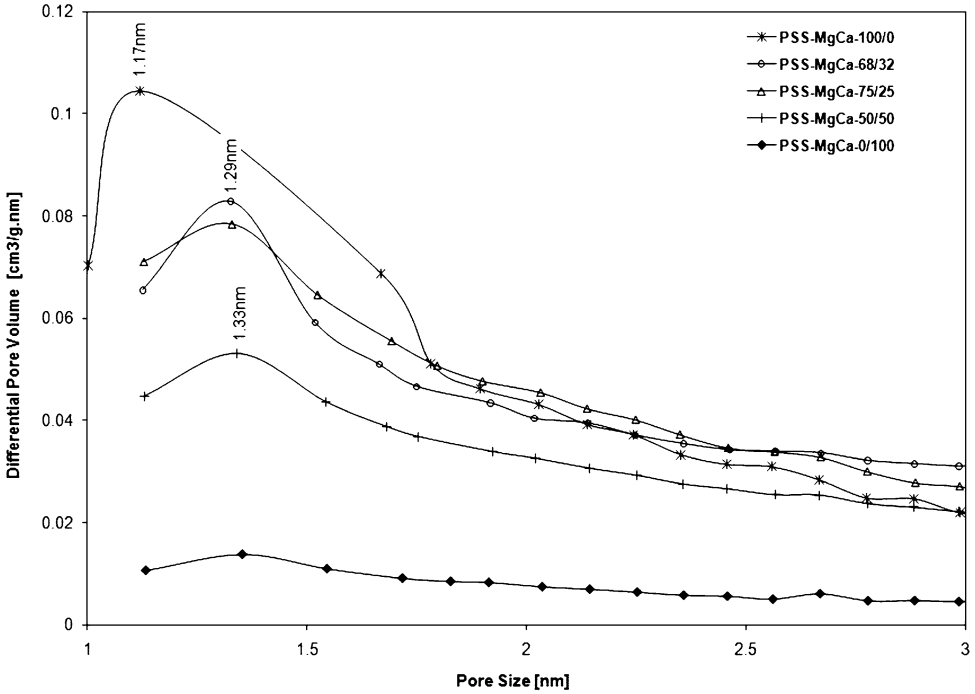

Fig. 7 Horvath–Kawazoe (HK) micropore size distribution for sorbents prepared with various Mg- and or / Ca- mol%

Table 3 Horvath-Kawazoe equation parameters (Larsen et al. 2000)

Species	Mag. susceptibility (m^3)	Polarizability (cm^2)	Diameter (nm)	Diameter at zero energy (nm)	Density (molec/cm^2)
Oxide ion	1.3×10^{-29}	2.5×10^{-24}	0.27	0.2369	1.4×10^{15}
Nitrogen	3.6×10^{-29}	1.76×10^{-24}	0.30	0.2574	6.71×10^{14}

the shape of isotherms and PSD of the rest of the samples (see Fig. 8). Further examination indicates that impregnation tend to increase the pores and shift the maximum pore peak to larger pore diameter. Thus for example, PSS-MgCa-100/0, PSS-MgCa-75/25, and PSS-MgCa-50/50, which exhibited narrow pore size range, tend to get a broader pore size distribution with larger maximum pore diameter located at 3.7, 3.5, and 25.4 nm respectively. This resulted in the increase of the pore volumes in that region and the total pore volume as a whole. With the exception of PSS-MgCa-100/0-KOH, the pore size was shifted to 3.7 nm but the total pore volume decreased. These findings indicate that PSS-MgCa-68/32-KOH sorbent porosity is more stable than the rest of the samples when a KOH impregnation is added.

3.4 Water stability

All the sorbents prepared and impregnate have been tested for their water stability by immersing the materials in the form of pellets into water at 23 °C for 24 h. These pellets are held together by the natural bonds coming into action when the paste or slurry is dried at 105 °C. It was observed that all the sorbents obtained did not soften, swell or disintegrate in water. It was also interesting to note that the samples impregnated with KOH did not show any pH change indicating that the KOH in the PSS-MgCa pore structure were stable and not dissolvable in water.

3.5 Desulfurization performance of the impregnate PSS-MgCa- sorbents

Figure 9a shows the up- and downstream concentration of SO_2 versus time for PSS-MgCa-sorbents with 8 wt% potassium hydroxide. Figure 9b shows the corresponding removal efficiencies [%] versus adsorbed amount of SO_2 in wt% (grams SO_2/grams sorbent).

When comparing the uptake of the impregnated sorbents at 50 % efficiency, it was observed that the uptake capacity was in the order of PSS-MgCa-68/32-KOH > PSS-MgCa-75/25-KOH > PSS- PSS-MgCa-50/50-KOH > PSS-MgCa-100/0-KOH. Among the impregnated samples with Mg and Ca, MgCa-68/32-KOH has a highest uptake at about 3 wt% where as MgCa-75/25-KOH has 2 wt% and MgCa-50/50-KOH has 1.8 wt%. Just for uptake comparison, the commercial media has about 0.5 wt% uptake (see Fig. 9) The results show that the uptake capacity of SO_2 is dependent on the Mg/Ca mol% and the pore structure parameters. The effects

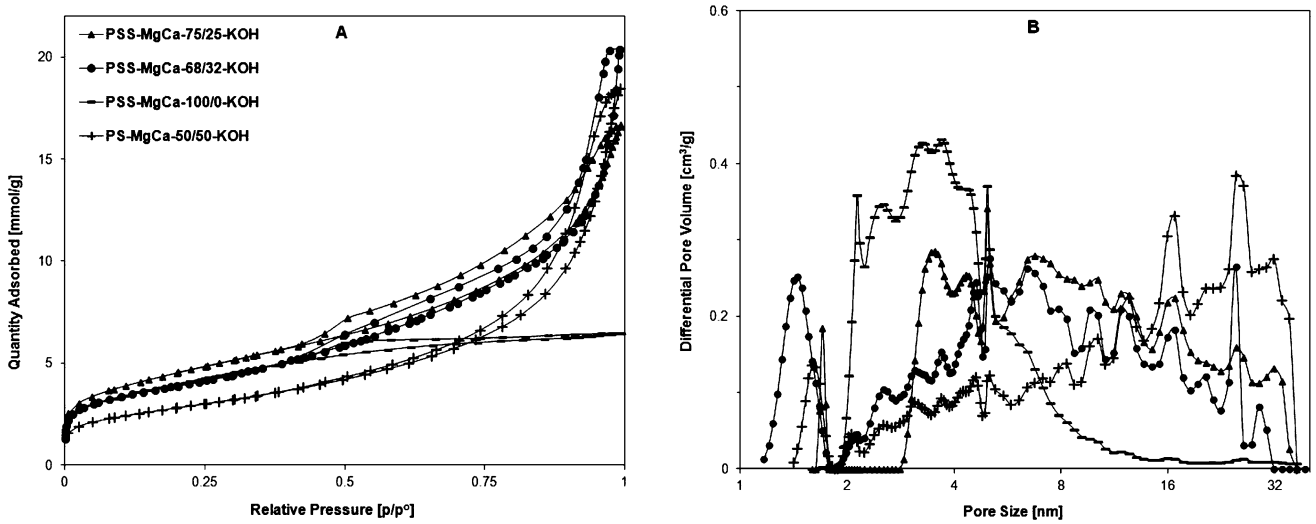

Fig. 8 Nitrogen adsorption-desorption isotherms (**A**) and (**B**) pore size distribution of PSS-MgCa-sorbents impregnated with 8 wt% KOH. PSD of the samples have been determined by N_2–Cylindrical Pores-Oxide surface model and assuming cylindrical pore geometry

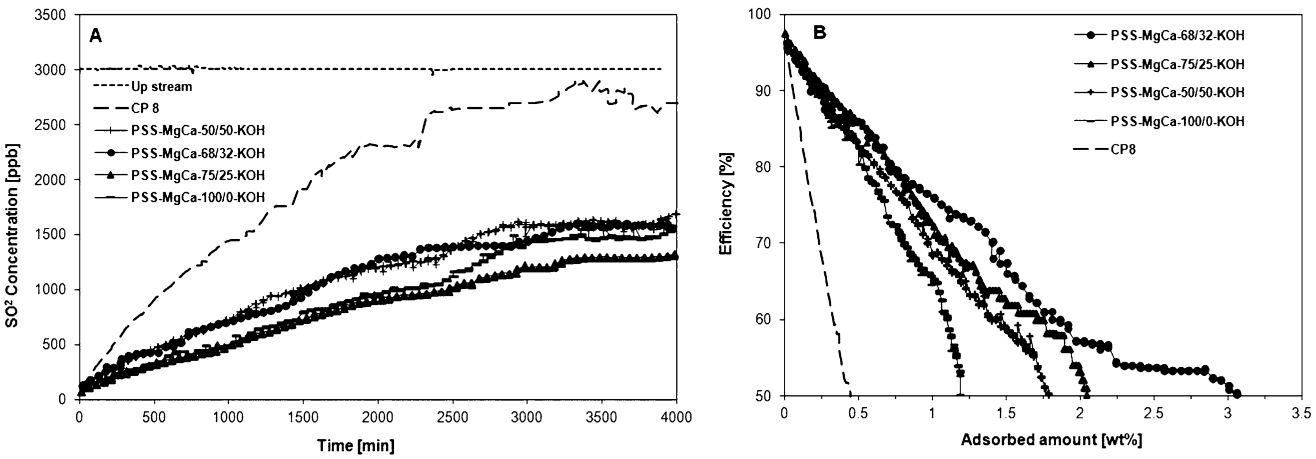

Fig. 9 Comparative performance of Sorbents impregnate with 8 wt% KOH

of porosity parameters on SO_2 uptake are further examined in the next section.

Although the sorbents prepared have calcium-magnesium silicates which are believed to have basic sites (Lin et al. 2003; Rodriguez et al. 2000) for SO_2 chemisorption at higher temperature, at room temperature however, no practical uptake has been reported (Ahmed and Attia 1998). As a result the sorbents with Ca mol% > 50 and 100 mol% Mg had been impregnated with potassium hydroxide as these materials show better porosity data. Thus the potassium hydroxide in the pore structure of the MgCa-Silica sorbent will provide the necessary basic site for acid-base reaction to occur at room temperature. On the moist-basic surface of borosilicate fibre filter, the following reaction has been reported (Hsu et al. 2007) and the same is expected to be dominant in the interior pores of MgCa-Silica sorbents as listed below.

$$SO_2 + KOH \leftrightarrow KHSO_3 \quad (2)$$

$$KHSO_3 + KOH \leftrightarrow K_2SO_3 + H_2O \quad (3)$$

3.6 Effect of pore structure on desulfurization performance

All the impregnated PSS-MgCa-sorbents have the same amount of potassium hydroxide content and it would be reasonable to expect a similar SO_2 uptake. The exceptional dynamic adsorption performance of PSS-MgCa-68/32-KOH must then be the results of the differences in the pore parameters between these PSS-MgCa-sorbents as shown in Fig. 10.

The relationship between specific surface area and micropore volume (V_{mic}) and SO_2 uptake capacities was plotted

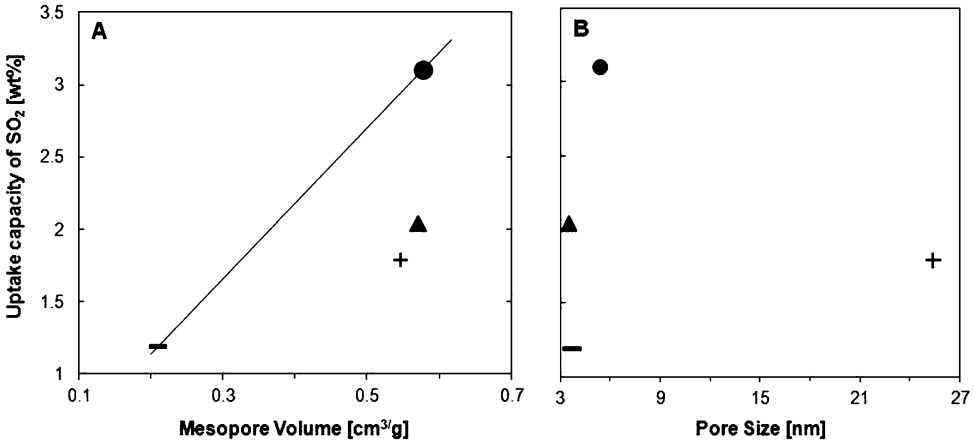

Fig. 10 Relationship between (**A**) the mesopore volume and dynamic SO_2 uptake capacity and (**B**) the pore size and dynamic SO_2 uptake capacity for impregnates samples and the commercial media CP 8; The filled circles represent PSS-MgCa-68/32-KOH (●), filled triangle represent PSS-MgCa-75/25-KOH (▲), plus represent PSS-MgCa-50/50-KOH (+) and filled rectangle represent PSS-MgCa-100/0-KOH (–)

and no correlation was observed. As a result, the effect of mesopore volume (V_{tot}–V_{mic}) has further been analysed.

Figure 10a and b depicts the relationships between the maximum mesopore size and the respective mesopore volume and the dynamic SO_2 uptake capacities for all MgCa-silica impregnate samples. Moreover, a high correlation between mesopore volume to SO_2 uptake was observed. Further, Fig. 10 indicates that although pore diameter itself does not show any strong relation, the combinations of mesopore diameter and high proportion of volume in that pore size region are important factors for SO_2 uptake. This can further be observed when comparing MgCa-silica sorbents with different ratios of Mg/Ca but with same content of potassium hydroxide. The PSS-MgCa-75/25-KOH and PSS-MgCa-100/0-KOH samples whose mesopore diameter is slightly smaller (∼ 3.5 and 3.7 nm) than that of PSS-MgCa-68/32-KOH (∼5.4 nm) and the same time have less mesopore volume exhibits low uptake capacity of SO_2. The mesopore diameter and volume and uptake capacity is in the order of MgCa-68/32 > MgCa-75/25 > MgCa-50/50 > MgCa-100/0. Furthermore, PSS-MgCa-75/25-KOH shows higher uptake capacity over PSS-MgCa-50/50-KOH even though the latter has larger mesopore pore diameter. This indicates that the larger mesopore volume is a major contributing feature for the enhanced uptake of PSS-MgCa-75/25-KOH.

This large uptake of PSS-MgCa-68/32-KOH can further be derived from a synergetic effect of the broad pore size distribution (1–32 nm). This bimodal pore system is vital for effective SO_2 removal as large mesopores diameters permits bulk diffusion and at the same time have micropore diameter for the trapping of the SO_2 molecule of diameter 0.4112 nm (Sun et al. 2011). The large mesopore volume of PSS-MgCa-68/32-KOH also allows for multiple SO_2 molecules collisions to occur. In interior pore system, statistically significant number of sufficiently energetic molecular collisions between the $[OH]^-$ anion on pore walls and SO_2 must occur before considerable chemical reactivity can be achieved and effective uptake of SO_2 obtained. The reaction product K_2SO_3 resides on the surface of the interior pore walls. Therefore having large proportion of pores in smaller pore diameter region will lead to reduced gas diffusion rate as more K_2SO_3 forms.

This will affect the media's ability to serve as an effective conduit for SO_2 gas molecules and for reaction product storage. It is likely that this was occurring in the case of PSS-MgCa-75/25-KOH whose efficiency was of same magnitude as the PSS-MgCa-68/32-KOH materials up until 80 % efficiency. Below this efficiency the K_2SO_3 crystals begin to inhibit diffusion as more crystals forms on the interior pore walls of PSS-MgCa-75/25-KOH. The scenarios mentioned above, along with the pore size data and mesopore volume, explained qualitatively the superior performance of PSS-MgCa-68/32-KOH. The situation above was also similar for the other impregnated samples.

4 Conclusion

Mg/Ca-silica sorbents have been prepared using sodium silicate and precipitated with various Mg/Ca molar ratios. Their adsorptive properties and performance have been determined by nitrogen adsorption/desorption and dynamic sulphur dioxide adsorption respectively. In addition, structural properties and morphology have been studied using X-ray diffraction and SEM.

The materials investigated are essentially amorphous. However, formation of crystalline compounds was traced in sorbents made with >50 mol% Ca, i.e. PSS-MgCa-50/50 and PSS-MgCa-0/100. These sorbents exhibited low specific surface area (S_{BET}) and total pore volume (V_{tot}). For sorbents with 100 mol% Mg (PSS-MgCa-100/0) a relatively higher S_{BET} and V_{tot} was found. Further, sorbents made with 68 mol% Mg and 32 mol% Ca (PSS-MgCa-68/32) and 75 mol% Mg and 25 mol% Ca (PSS-MgCa-75/25) exhibited even higher specific surface area and total pore volume.

All sorbents consisting of Mg/Ca-silica exhibited bimodal porosity (containing both micropores and mesopores). With high amount of micropore area and volume observed in sorbents made with $\geq$ 75 mol% Mg whereas PSS-MgCa-68/32 shows relatively high mesopore area and volume. The NLDFT PSD of sorbents with 68 mol% Mg and 32 mol% Ca (PSS-MgCa-68/32) exhibits wide pore size range of 1 to 32 nm whereas sorbent made with 75 mol% Mg and 25 mol% Ca together with 50 mol% Mg and 50 mol% Ca shows narrow pore size range of 1 to 5 nm. Effect of impregnation on the PSS-MgCa-68/32 porosity was not significant but strong effect was observed in the rest of the samples.

The desulfurization performance behavior was evaluated for PSS-MgCa sorbents with 8 wt% potassium hydroxide, all of which had ability to adsorbed SO_2. The highest SO_2 uptake corresponds to PSS-MgCa-68/32-KOH. The combined synergetic effect between large mesopore diameter and extensive mesopore volumes or channels is a key factor in achieving a large SO_2 uptake.

The impregnated samples (PSS-MgCa-68/32-KOH, PSS-MgCa-75/25-KOH and PSS-MgCa-50/50-KOH) show a promise of delivering high uptake of SO_2 making them suitable for demanding application.

Acknowledgements We are grateful to Svenska Aerogel AB for providing the sorbents used in this study and to Ann-Charlotte at Camfil AB for performing the challenge measurements. We are also grateful to Dr. Alfonso E. Garcia-Bennet and Dr. Rambabu Atluri at the Ångström Laboratory, Uppsala University for providing the adsorption instrument and for the open research atmosphere and fruitful discussions.

References

Ahmed, M.S., Attia, Y.A.: Multi-metal oxide aerogel for capture of pollution gases from air. Appl. Therm. Eng. **18**, 787–797 (1998)

Ashrae Standard I45.I Laboratory Test Method for Assessing the Performance of Gas-Phase Air-Cleaning Systems: Loose Granular Media (2008)

Bonneviot, L., Beland, F., Danumah, C., Giasson, S., Kaliaguine, S.: Mesoporous Molecular Sieves: Proceedings of the First International Symposium. Studies in Surface Science and Catalysis, vol. 117, pp. 143–154 (1998)

Brew, D.R.M., Glasser, F.P.: Synthesis and characterisation of magnesium silicate hydrate gels. Cem. Concr. Res. **35**, 85–98 (2005)

Ciesielczyk, F., Krysztafkiewicz, A., Jesionowski, T.: Physicochemical studies on precipitated magnesium silicates. J. Mater. Sci. **42**, 3831–3840 (2007)

Finlayson-Pitts, B.J., Pitts, J.N.: Atmospheric Chemistry: Fundamentals and Experimental Techniques. Wiley, New York (1986)

Horvath, G., Kawazoe, K.: Method for the calculation of effective pore size distribution in molecular sieve carbon. J. Chem. Eng. Jpn. **16**, 470 (1983)

Hsu, Y.M., Kollett, J., Wysocki, K., Wu, C.Y., Lundgren, D.A., Birky, B.K.: Positive artifact sulfate formation from SO_2 adsorption in the silica gel sample used in NIOSH method 7903. Environ. Sci. Technol. **41**, 6205–6209 (2007)

Iler, R.K.: The Chemistry of Silica, Solubility, Polymerization, Colloid and Surface Properties, and Biochemistry, pp. 558–559. Wiley, New York (1979)

Jennings, M.H., Bullard, J.W., Thomas, J.J., Andrade, J.E., Chen, J.J., Scherer, G.W.: Characterization and modeling of pores and surfaces in cement paste: correlations to processing and properties. J. Adv. Concr. Technol. **6**(1), 5–29 (2008)

John, D., McCarthy, J.F., Samet, J.M.: Indoor Air Quality Handbook. McGraw-Hill, New York (2000) pp. 271

Kruk, M., Jaroniec, M.: Adsorption study of surface and structural properties of MCM-41 materials of different pore sizes. J. Phys. Chem. B **101**, 583–589 (1997)

Larsen, G., Lotero, E., Marquez, M.: Amine dendrimers as templates for amorphous silicas. J. Phys. Chem. B **104**, 4840–4843 (2000)

Lin, R.B., Shin-Min, S., Chiung-Fang, L.: Characteristics and reactivities of $Ca(OH)_2$/silica fume sorbents for low-temperature flue gas desulfurization. Chem. Eng. Sci. **58**, 3659–3668 (2003)

Lu, G.Q.: Nanoporous Materials: Science and Engineering. Imperial College Press, London (2004) pp. 874

Odler, I.: The BET-specific surface area of hydrated Portland cement and related materials. Cem. Concr. Res. **33**, 2049–2056 (2003)

Pierre, A.C., Pajonk, G.M.: Chemistry of aerogels and their applications. Chem. Rev. **102**, 4243–4265 (2002)

Renedo, M., Fernández, J.J.: Preparation, characterization, and calcium utilization of fly ash/$Ca(OH)_2$ sorbents for dry desulfurization at low temperature. Ind. Eng. Chem. Res. **41**, 2412–2417 (2002)

Rouquerol, F., Rouquerol, J., Sing, K.: Adsorption by Powders & Porous Solids Principles, Methodology and Applications, pp. 176–205, 362–370. Academic Press, San Diego (1996)

Rodriguez, J., Jirsak, T., Freitag, A., Larese, J.: Interaction of SO_2 with MgO (100) and Cu/MgO (100): decomposition reactions and the formation of SO_3 and SO_4. J. Phys. Chem. B **104**, 7439–7448 (2000)

Ryoo, R., Kim, J.M., Ko, C.H., Shin, C.H.: Disordered molecular sieve with branched mesoporous channel network. J. Phys. Chem. **100**, 17718–17721 (1996)

Schweitzer, P.A.: Handbook of Separation Techniques for Chemical Engineers. McGraw-Hill, New York (1979) pp. 238

Sun, F., Gao, J., Zhu, Y., Qin, Y.: Mechanism of SO_2 adsorption and desorption on commercial activated coke. Korean J. Chem. Eng. **28**(7), 1025–1031 (2011)

Taspinar, O.O., Ozgul-Yucel, S.: Lipid adsorption capacities of magnesium silicate and activated carbon prepared from the same rice hull. Eur. J. Lipid Sci. Technol. **110**, 742–746 (2008)

Yang, R.T.: Sorbents: Fundamental and Applications, pp. 3–7. Wiley, Hoboken (2003)

Zheng, F., Addleman, R.S., Aardahl, L.C., Fryxell, G.E., Brown, D.R., Zemanian, T.S.: In: Fryxell, G.E., Guozhong, C. (eds.) Environmental Applications of Nanomaterials: Synthesis, Sorbents and Sensors, pp. 285–306. Imperial College Press, London (2007)